A New Aerosol Dry Deposition Model for Air Quality and Climate Modeling

Jonathan E. Pleim[1], Limei Ran[2], Rick D. Saylor[3], Jeff Willison[4], and Francis S. Binkowski[5]

[1]U.S. Environmental Protection Agency, Research Triangle Park, North Carolina, USA, pleim.jon@epa.gov

[2]U.S. Department of Agriculture, Natural Resources Conservation Service, Greensboro, North Carolina, USA, limei.ran@usda.gov

[3]Air Resources Laboratory, National Oceanic and Atmospheric Administration, Oak Ridge, Tennessee, USA, rick.saylor@noaa.gov

[4]U.S. Environmental Protection Agency, Research Triangle Park, North Carolina, USA, willison.jeffrey@epa.gov

[4]Institute for the Environment, University of North Carolina at Chapel Hill, Chapel Hill, North Carolina, USA, francisbinkowski@gmail.com

Key Points

- New aerosol deposition velocity model agrees better with observations than current models
- Impaction on microscale obstacles such as leaf hairs is key process
- New aerosol deposition velocity model increases dry deposition of $PM_{2.5}$ compared to the current CMAQ model

Abstract

Dry deposition of aerosols from the atmosphere is an important but poorly understood and inadequately modeled process in atmospheric systems for climate and air quality. Comparisons of currently used aerosol dry deposition models to a compendia of published field measurement studies in various landscapes show very poor agreement over a wide range of particle sizes. In this study, we develop and test a new aerosol dry deposition model that is a modification of the current model in the Community Multiscale Air Quality (CMAQ) model. The new model agrees much better with measured dry deposition velocities across particle sizes. The key innovation is the addition of a second inertial impaction term for microscale obstacles such as leaf hairs, microscale ridges, and needleleaf edge effects. The most significant effect of the new model is to increase the mass dry deposition of the accumulation mode aerosols in CMAQ. Accumulation mode mass dry deposition velocities increase by almost an order of magnitude in forested areas with lesser increases for shorter vegetation. Peak $PM_{2.5}$ concentrations are reduced in some forested areas by up to 40% in CMAQ simulations. Over the continuous United States, the new model reduced $PM_{2.5}$ by an average of 16% for July 2018 at the Air Quality System monitoring sites. For summer 2018 simulations, bias and error of $PM_{2.5}$ concentrations are significantly reduced, especially in forested areas.

Plain Language Summary

Aerosol dry deposition is an important sink for atmospheric particles that are a health hazard and a significant climate forcer. Uncertainties in modeling aerosol dry deposition hamper accurate predictions of air quality and climate. A new aerosol dry deposition

model is developed that better agrees with observations of aerosol dry deposition velocity for a variety of vegetation such as forests, grasslands, and water surfaces. This improved aerosol dry deposition model when incorporated into air quality and climate models will improve the accuracy of model predictions.

1. Introduction

The lifetime and fate of aerosols in the atmosphere are strongly influenced by wet and dry deposition processes. Thus, the representation of these processes are key elements of atmospheric models for air quality, climate, and ecosystem impacts. The uncertainties in modeling aerosol dry deposition contribute significantly to the uncertainties and errors in direct and indirect radiative forcing that have been identified as some of the most uncertain processes in global climate modeling (IPCC, 2021). Currently, there are a wide variety of aerosol dry deposition models used in atmospheric modeling systems that reflect a great degree of uncertainty. Recently, there have been several studies that compiled observations of aerosol dry deposition in a variety of environments for particle sizes that range from 10s of nanometers to 10s of microns (Saylor et al., 2019; Emerson et al., 2020; Farmer et al., 2021). Saylor et al. (2019) showed that models differ greatly from the observations especially for forested landscapes. Model errors compared to observations vary among different models and overpredict in some size ranges while underpredicting in other size ranges.

Most size-resolved aerosol dry deposition models used in large-scale air quality and climate models are combinations of mathematical algorithms representing the major processes involved in aerosol deposition as presented by Slinn (1982). All these processes have strong dependencies on particle size and their combination yields a relationship with the dry deposition velocity as a function of particle diameter (i.e., $V_d(d_p)$). However, since the models in use today have been shown to not agree well with consensus of observations, particularly for forests, these models need to be re-examined and revised. Key questions include: Can the parameterizations of the major processes be revised to improve results or are there key processes that have been neglected?

The focus of this paper is to address uncertainties in the current aerosol dry deposition modeling and to propose a new model that builds on current forms but includes a key new process that greatly improves agreement with the consensus of observations. Section 2 describes physical processes controlling dry deposition modeling. The proposed new model is described in Section 3. Evaluation of the new model against measurements and discussion are presented in Section 4. Section 5 presents the implementation and evaluation of the new model in the Community Multiscale Air Quality (CMAQ) model (Byun and Schere, 2006) for regional applications. Concluding remarks and future work are given in Section 6.

2. Physical processes in modeling dry deposition

The concept of dry deposition velocity (V_d) is that surface flux (F) of a trace atmospheric constituent is directly proportional to its concentration (C) just above the surface as:

$$F = V_d \times C \tag{1}$$

In this way physical and dynamical processes can be isolated from chemical processes. The principal processes involved in aerosol dry deposition include gravitational settling, Brownian diffusion, surface impaction, surface interception, and rebound. All these processes are functions of particle diameter (d_p) and become more effective as particle size increases except Brownian diffusion which is most effective for ultrafine particles. Aerosol particles are transported from the air to the surface simultaneously by turbulent fluxes and gravitational settling. The gravitational settling velocity (V_g) results from a balance of gravitational and viscous drag forces as (Stokes, 1851):

$$V_g = \frac{g \rho_p d_p^2 C_c}{18\mu} \tag{2}$$

where g is the gravitational acceleration, ρ_p is the particle density, μ is the dynamic viscosity of air and C_c is the Cunningham slip correction factor for small particles (Cunningham, 1910). The turbulent fluxes are modeled similarly to gas dry deposition fluxes as combinations of resistances. Flux through the turbulent surface layer is represented by aerodynamic resistance R_a which is the same for gases and aerosols (Pleim and Ran, 2011). However, since the no-slip condition for viscous fluids requires that the velocity is exactly zero at the boundary, there is a very thin quasi-laminar sublayer adjacent to all surfaces. For gases, molecular diffusion across this layer is so efficient that the resistance presented by this layer R_b is rarely the limiting factor relative to R_a and surface resistances. For aerosol, however, R_b is usually the most limiting resistance because diffusion of particles (Brownian diffusion) is much slower than molecular diffusion. Gravitational settling and turbulent fluxes are combined to compute aerosol deposition velocity as (Venkatram and Pleim, 1999),

$$V_d = \frac{V_g}{1-exp\left(-V_g(R_a+R_b)\right)} \quad (3)$$

The quasi-laminar boundary layer resistance can be expressed in terms of collection efficiencies *E* (Slinn, 1982),

$$R_b = \frac{1}{LAI \cdot u_*(E_B+E_{im}+E_{in})R} \quad (4)$$

where *LAI* is leaf area index, u_* is the friction velocity, E_B is Brownian diffusion collection efficiency, E_{im} is impaction collection efficiency, and E_{in} is interception collection efficiency. Particles that encounter a surface can either stick or bounce off which is represented by the rebound factor *R* in Equation 4 that mostly affects the largest particles. Most recent aerosol dry deposition models follow the formulations for the collection efficiencies proposed by Slinn (1982) with a variety of modifications and extensions.

Aerosol deposition to vegetated areas is particularly complex and difficult to model given the wide array of vegetation types with different canopy morphologies and leaf shapes. Figure 1 shows that several models, including the models currently used in CMAQ, the Comprehensive Air quality Model with extensions (CAMx) (ENVIRON, 2020), the Goddard Earth Observing System model with Chemistry (GEOS-Chem) (Bey et al., 2001), a Unified Regional Air-quality Modeling System (AURAMS) (Gong et al., 2006), and the Global Environmental Multi-scale model - Modelling Air quality and CHemistry (GEM-MACH) (Gong et al., 2015), cannot well represent aerosol deposition for all particle sizes at evergreen needleleaf forest sites. The current CMAQv5.3 model, which is a modified version of the earlier CMAQ model described by Pleim and Ran (2011), and the Zhang (2001) model that is used in CAMx, AURAMS, GEM-MACH and

GEOSChem both seem to have the wrong shape with minimum V_d at around 2-3 μm while the measurements indicate minimum at about 0.1 – 0.2 μm. Note that there are two curves for the CMAQv5.3 model because its formulation includes a function of convective velocity scale (w_*). The models of Petroff and Zhang (2010) and Zhang and Shao (2014) have minimum values at much smaller sizes with the Petroff and Zhang (2010) model agreeing well with the aggregate observations in the less than 0.2 μm size range. The recent model described by Emerson et al. (2020) also agrees well with the size of minimum V_d for forest observations as will be shown and discussed in Section 4. However, none of the models seem to capture the rapid increase in deposition velocity seen in the observations from 0.2 to about 0.5 μm and the plateau from 0.5 to about 5 μm. Clearly, the models as currently formulated are not able to produce the S-shaped curve of the observation consensus.

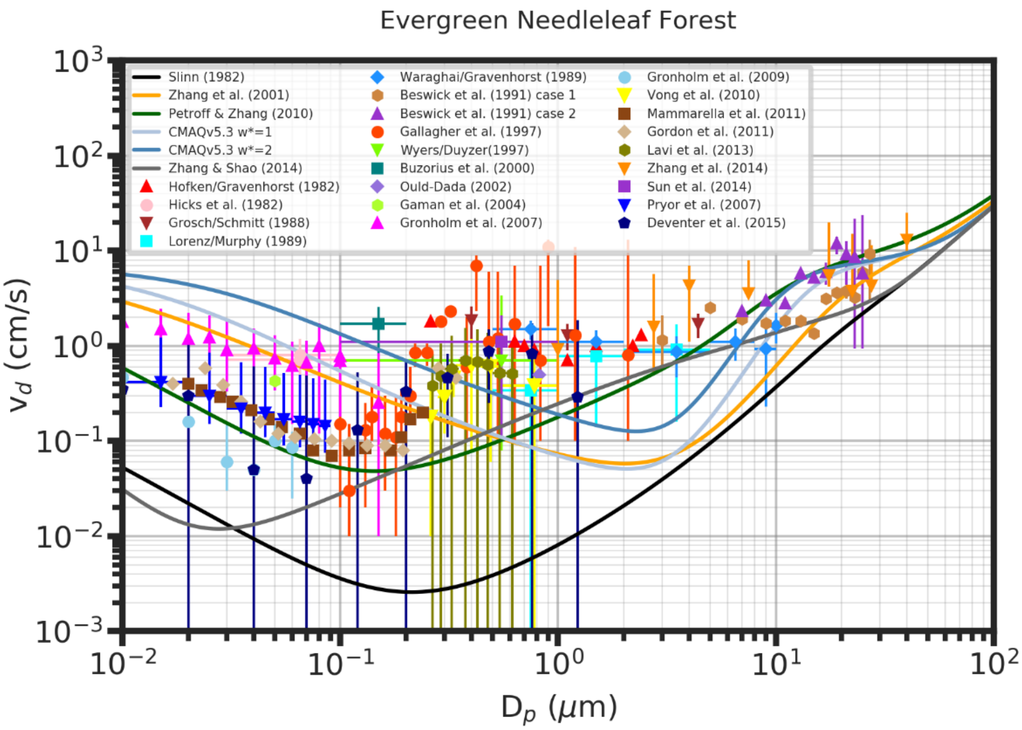

Figure 1. Measured aerosol dry deposition velocities from literature as functions of particle size for evergreen needleleaf forest. Symbols represent median values with error bars that represent estimated uncertainty, usually inter-quartile range. The lines show predictions by various models assuming u_* = 0.4 m/s. Adapted from Saylor et al. (2019).

Several recent studies have shown that leaf surface texture and leaf shape have significant influence on aerosol dry deposition. For example, Chen et al. (2017) found that the needle-shaped leaves of conifers were more effective in general than broad leaves at $PM_{2.5}$ (particulate matter with an effective aerodynamic diameter less than 2.5 μm) aerosol dry deposition. They also found that broad leaf species with more grooves or hairs tended to increase deposition. Several other studies involving both field measurements and wind-tunnel experiments also showed increased deposition for leaves with dense hairs, ridges, grooves or thick epicuticular wax layers (e.g., Weerakkody et al, 2017; Chiam et al., 2019; Leonard et al, 2016). Perini et al. (2017) also found enhanced fine aerosol deposition on leaves with thick cuticular waxes but less so for hairy leaves. By measuring aerosols accumulating on 22 species of trees and 25 shrubs, Sæbø et al. (2012) found that leaf properties such as hair and wax cover enhanced aerosol deposition among the broad-leaf species while needle-leaf species were also among the highest aerosol collecting species. Beckett et al. (2000) found greater deposition of 1 μm aerosols on pine needles than broad flat leaves in wind-tunnel studies. They noted that deposition was well correlated with Stokes number which is inversely proportional to the characteristic leaf size which for needles was on the order of 1 mm and about 5 cm or more for broad leaves. Zhang et al. (2021) tested the effects of leaf hair (trichome) density, leaf aspect ratio, petiole (leaf stem) length, and leaf fractal deviation on $PM_{2.5}$ deposition. They found higher trichome density, lower aspect ratio, shorter petiole, and greater leaf fractal deviation all increase $PM_{2.5}$ dry deposition velocities.

3. New model description

The new model, which is intended to replace the current aerosol dry deposition scheme in CMAQ, follows the same general framework that was originally proposed by Slinn (1982) as shown in equations 3 and 4. The aerodynamic resistance is unchanged from the current CMAQ model and is the same for gases and aerosols (Pleim and Ran, 2011). Unlike the current scheme, calculation of the quasi-laminar boundary layer resistance R_b differs for the vegetated and non-vegetated parts of each grid cell. The most important change is to the parameterization of the impaction collection efficiency where a term is added to better represent the shape of the deposition velocity curve for vegetated areas.

3.1 Vegetated areas

For the vegetated fraction of each grid cell the R_b is weighted by LAI to account for the total leaf surface area density available for deposition as shown in Equation 4. The Brownian collection efficiency E_B follows Slinn (1982) as:

$$E_B = \left(\frac{C_v}{C_d}\right) Sc^{-2/3} \quad (5)$$

where *Sc* is the Schmidt number defined as the ratio of the kinematic viscosity of air divided by the Brownian diffusivity $Sc = {}^{\nu}/_{D_B}$ and c_v/c_d is the ratio of viscous drag to total drag which we specify as 1/3 as deduced by Chamberlain (1966) for grass.
A key innovation in the new model to better fit observed dry deposition velocities by particle size is to represent the impaction efficiency by two terms to account for the effects of macroscale and microscale obstacles. Impaction efficiency E_{im} is generally expressed as a function of Stokes number *St*, which describes the tendency of a particle to follow fluid flow around obstacles. In the quasi-laminar sub-layer, the relevant flow velocity is given by the turbulent friction velocity u_* which is the characteristic velocity of turbulent eddies in the turbulent layer above the quasi-laminar sub-layer. Therefore, for vegetated surfaces, *St* is defined as,

$$St = \frac{V_g u_*}{gA} \quad (6)$$

where *A* is the characteristic dimension of the obstacles. For the new model, we define St_l and St_h using different obstacle characteristic dimensions for the leaf scale A_l and microscale A_h representing features such as leaf hairs (trichomes) or other microscale roughness on leaves. Thus, E_{im} is given as,

$$E_{im} = (1 - f_{micro})\frac{St_l^2}{1+St_l^2} + f_{micro}\frac{St_h^2}{1+St_h^2} \quad (7)$$

where f_{micro} is the fraction of total impaction due to the microscale features. The concept of using macro and microscale obstacle size scales was introduced by Slinn (1982) for interception processes. Slinn (1982) speculated that the microscale obstacles would probably not be relevant for impaction because the vegetative hairs or other microscale obstacles such as cobwebs would be deflected by the flow and not be significant collectors by impaction. However, testing the two-term approach for both interception and impaction showed that expressing impaction as in Equation 7 matched the size dependent deposition velocities, especially for forests, much better than using a similar expression for interception only. Note that both f_{micro} and A_h are very uncertain parameters. Slinn (1982) suggested f_{micro} = 1% but we found better fit to observations with a slight reduction to f_{micro} = 0.8%. The microscale characteristic obstacle scale is specified by land use category (LUC) such that A_h = 0.5 μm for needleleaf forest and grasslands and A_h = 1.0 μm for deciduous forest. The macroscale characteristic obstacle scale is also specified by LUC with values ranging from 0.5 to 10 mm (Table 1).

The third collection efficiency in Equation 4 is interception. Interception is postulated as capture that occurs when a particle comes within a particle radius of a surface or obstacle. However, the physical basis of this process is less well defined than the Brownian or impaction processes. Including interception efficiency as recommended by Slinn (1982) had very little effect in the new model. Therefore, in the new model the interception collection efficiency is not used.

Table 1. Key parameters for new aerosol dry deposition model over different landscapes

LU Type	U_* (m/s)	LAI	f_v	f_{micro}	A_l (mm)	A_h (μm)
Needleleaf forest	0.4	5	93	0.008	2	0.5
Broadleaf forest	0.4	5	93	0.008	10	1.0
Grassland	0.3	2	95	0.002	0.5	0.5
Water	0.2	0	0	NA	NA	NA

3.2 Non-vegetated areas

For non-vegetated areas the definition of E_B is the same as for vegetated areas but the E_{im} is different,

$$E_{im} = 10^{-3/St} \tag{8}$$

where,

$$St = \frac{\rho_a V_g u_*^2}{g\mu} \tag{9}$$

These are the formulations recommended by Slinn (1977) for smooth surfaces where ρ_a is the air density. For water surfaces, the effects of whitecaps (breaking waves) are included in an additional term in the E_B expression,

$$E_B = (1 - f_{wc})\left(\frac{C_v}{C_d}\right) Sc^{-2/3} + f_{wc}\frac{u_*}{U_{10}} \tag{10}$$

as suggested by Pryor (1999) following Hummelshøj et al. (1992) where U_{10} is the windspeed at 10 m above the surface. Note that the more complex form in Pryor (1999) was not used because the term describing the particle capture by spray droplets is always much smaller than the u_*/U_{10} term. The effects of whitecaps increase rapidly with increasing windspeed as whitecaps cover more of the water surface. While most models parameterize the whitecap surface fraction f_{wc} as a function of windspeed, we follow Albert et al. (2016) who developed a parameterization based on satellite whitecap fraction data, that is also a function of water surface temperature T_{ws} in Celsius and U_{10} is in m/s,

$$f_{wc} = a(b + U_{10})^2 \quad (11)$$

where
$$a = a_1 + a_2 T_{ws} + a_3 {T_{ws}}^2$$
$$b = b_1 + b_2 T_{ws}$$

and a_1 = 8.46 x 10^{-5}, a_2 = 1.63 x 10^{-6}, a_3 = -3.35 x 10^{-8}, b_1 = 3.354, and b_2 = -0.062.

Another new modification is for the non-vegetated parts of urban LU categories where R_b is weighted by building area index (*BAI*). The rationale for this is that buildings add significant surface area in urban landscapes that is not accounted for by LAI or otherwise. An initial estimate is $BAI = (4\,\lambda_f + 1)/(1-f_v)$, where λ_f is frontal area density of building surfaces and f_v is the vegetated fraction of the grid cell. The logic for this is that the total building surface area is four times the frontal area. For applications where detailed building data is not included, default values of *BAI* are specified by landuse category. For example, *BAI* is specified as 1.8, 2.0, and 2.3 for the National Land Cover Database (NLCD) categories of low intensity developed, medium intensity developed, and high intensity developed, respectfully. For all other non-developed categories, *BAI* is set to 1. Thus, for unvegetated portions of urban grid cells R_b is defined as,

$$R_b = \frac{1}{BAI \cdot u_*(E_b + E_{im})} \quad (12)$$

Note that particle rebound effects are not considered (R=1) because only the largest particles are affected and there is much variation by composition, RH, surface type, and windspeed. Grid cell deposition velocity is the combination of the vegetated and non-vegetated parts,

$$V_d = f_v V_{dveg} + (1 - f_v) V_{dnoveg} \quad (13)$$

4. New model evaluation

The new model is evaluated against aerosol dry deposition measurements over different landscapes. The performance of the new approach is also discussed in terms of the enhanced processes.

4.1 Comparison to measurements

Following several recent papers (Saylor et al., 2019; Emerson et al., 2020; Farmer et al., 2021), we compile aerosol dry deposition measurements by particle size for various surface types from the published literature to compare to aerosol dry deposition models. Figure 2 shows the same data for evergreen needleleaf forest as figure 1 with the addition of the new model described here as well as the recent model described by Emerson et al. (2020). The parameter values for the model runs for each land use type are shown in Table 1. The new model, designated *New CMAQ*, is the only one that shows the increase of V_d in the 0.2 – 0.6 μm range and the plateau from about 0.6 μm to 6 μm. Compared to the CMAQv5.3 model, the new model substantially reduces the underprediction of V_d from about 0.5 – 5.0 μm. This has profound effects on dry deposition and concentration of $PM_{2.5}$ as will be shown in Section 5. The Emerson model generally fits the data very well since it was developed through changes to six empirical coefficients and exponents in the Zhang et al (2001) parameterization to optimize agreement with the needleleaf forest observation data. However, as shown in Figures 2 and 3, the Emerson model does not replicate the s-shaped curve suggested by the observations for needleleaf and broadleaf forest through the 0.1 – 5.0 μm range as well as the new model.

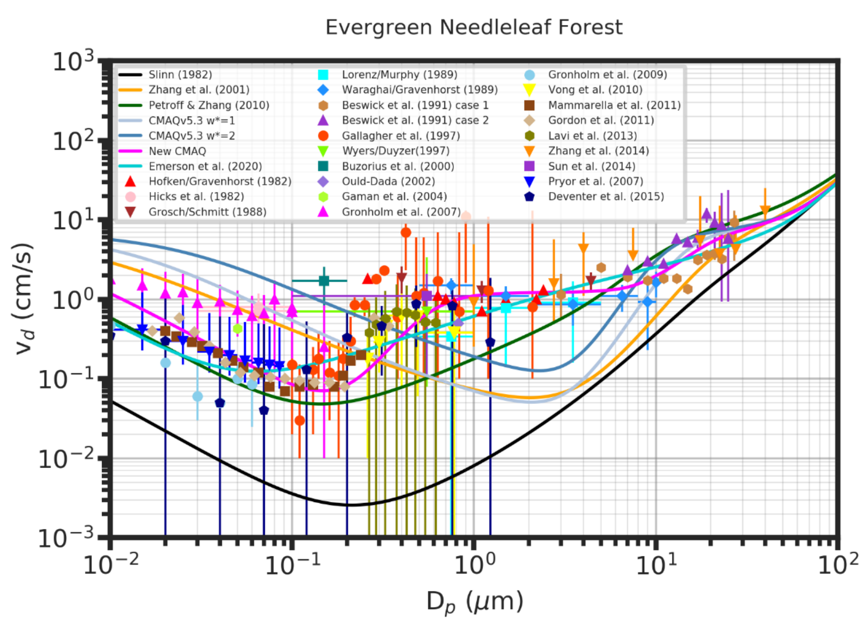

Figure 2. Measured aerosol dry deposition velocities from literature as functions of particle size for evergreen needleleaf forest. Symbols represent median values with error

bars that represent estimated uncertainty, usually inter-quartile range. The lines show predictions by various models assuming u_* = 0.4 m/s including the new model (new CMAQ) in magenta and the recent Emerson et al. (2020) model in turquoise. .

There are not as many measurement studies in the literature for other landuse/vegetation types. Figure 3 shows the observation data and models for deciduous broadleaf forest. The consensus of dry deposition measurements to broadleaf forests suggests a similar shape to the V_d vs d_p curve where there is an increase of V_d in the approximately 0.2 to 0.6 μm range with a plateau up to about 6 μm. Again, the new model is the only one that replicates the shape of this curve and does not greatly underestimate V_d in the 0.5 - 4.0 μm range.

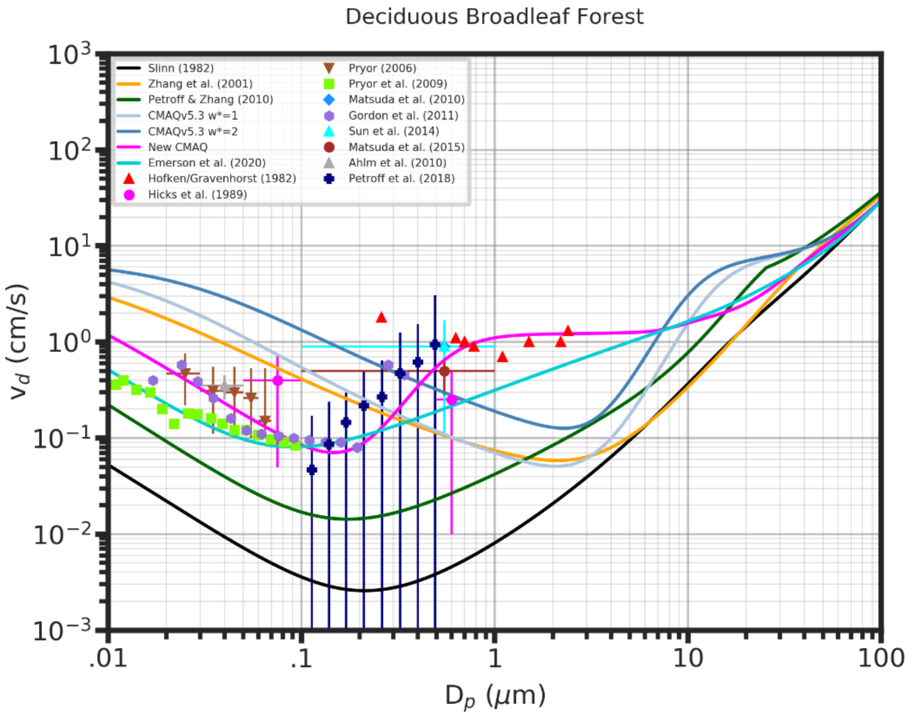

Figure 3. Same as figure 2 but for deciduous broadleaf forest.

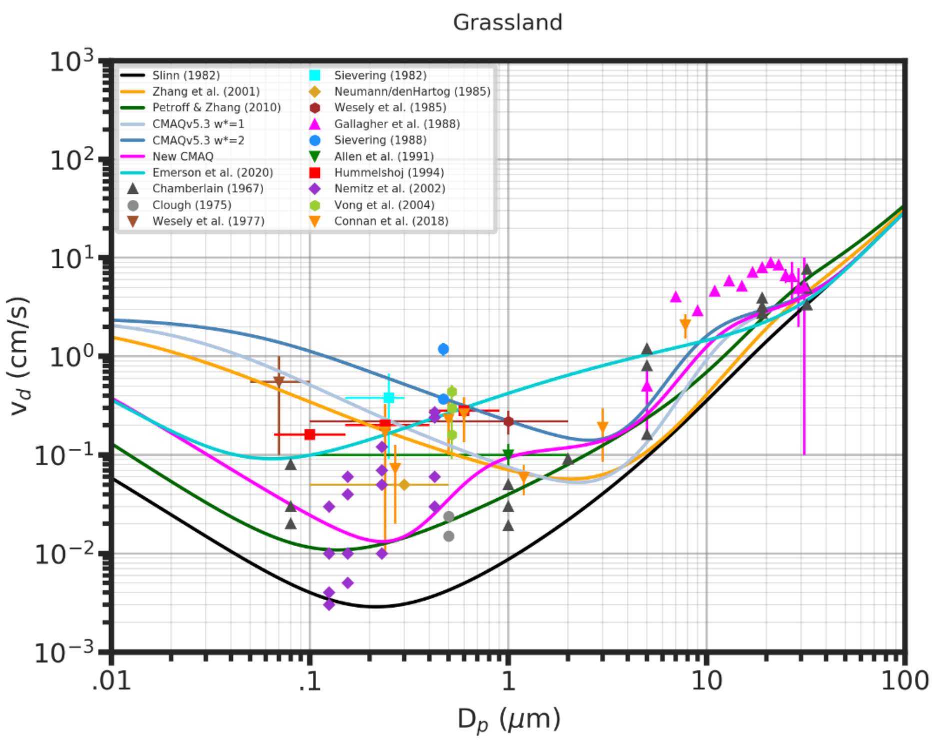

Figure 4. Same as figure 2 but for grasslands and u_* = 0.3 m/s.

Figure 4 shows the new model and other models for grasslands compared to measurements. While there are a lot of measurements for grasslands, there seems to be much less consensus among them, even within the same studies, than for forests. With the degree of scatter in the measurements there isn't clear guidance for parameter selection. While the rationale for microscale impaction may also apply to grass since grass leaves often have leaf hairs or trichomes and serrated edges, the evidence from the measurements is less clear. Therefore, the parameter values selected for the microscale impaction scaling factor f_{micro} are set to smaller values (see Table 1) than for forests, which seem to better fit with the measurements. Running box models on an hourly or sub-hourly basis using detailed field measurements may add some clarity to model performance and refinement of parameters.

The large scatter among the reported measurements for grassland is likely due the variety of grass species which can have very different characteristics including length. For example, the measurements reported by Vong et al. (2004) were made over rye grass 0.75 - 1 m tall, Allen et al. (1991) measured deposition to short grass of 3 – 7 cm in length, Conan et al. (2018) used artificial grass, and Nemitz et al. (2002) measured in a moorland which is characterized by hummocks and hollows with vegetation including peat moss (Sphagnum) and several species of tall grasses.

Virtually all studies found strong dependences of V_d on u_* with V_d increasing with increasing u_* (Pryor et al., 2008). Some have suggested that V_d/u_* is a more robust quantity for analysis and comparison (e.g., Conan et al., 2018) but many studies did not report this. Zhang et al. (2014) measured dry deposition velocities of dust particles (1 – 40 μm) in a wind tunnel at various wind velocities over different surfaces. To simulate deposition to trees, evergreen branches were planted in the test section surface. The new model set up for evergreen needleleaf forest is shown (Figure 5) to compare well to the tree wind tunnel experiments at three windspeeds with measured friction velocities of 0.24, 0.5, and 1.06 m/s.

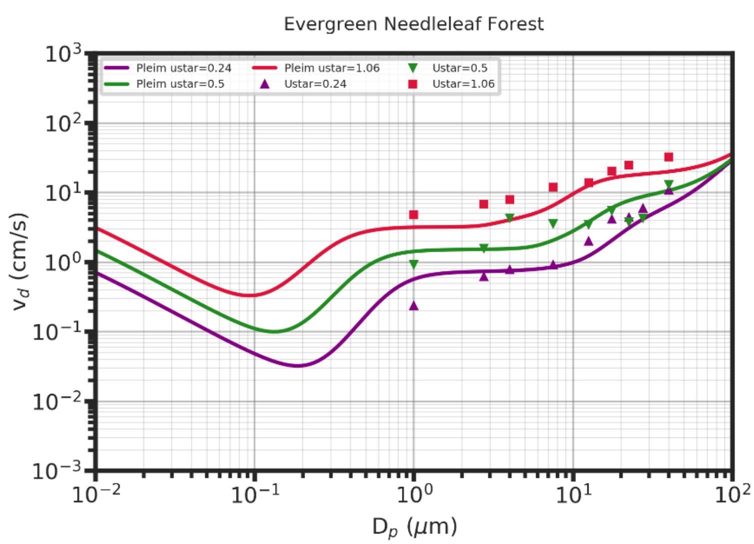

Figure 5. New model compared to wind tunnel experiments for tree surfaces (Zhang et al. 2014) at three friction velocities.

Figure 6 shows models compared to field measurements for water surfaces. Most of the measurements over water show that dry deposition velocities are much lower in the accumulation size range than for vegetated surfaces. The measurements by Sievering (1981) seem to be outliers with much higher deposition velocities in the 0.15 – 1 μm range. These measurements, which used the momentum gradient technique that assumes similarity between aerosol fluxes and momentum fluxes, can be particularly uncertain when the surface has bluff bodies such as waves than can induce form drag on momentum flux. The other outlier study is by Zhang et al. (2014) which is a wind tunnel study where dry deposition velocity is estimated by particle dynamic analysis (PDA). The measurements over water in the wind tunnel were found to agree quite well with the Slinn and Slinn (1980) (SS80) model for three different friction velocities when R_b is set to zero (Zhang et al., 2014, Figure 11). The authors hypothesize that this is due to waves and spray droplets. However, given the dramatic dissimilarity from most of the other studies, there could be an issue of scaling wave-wind dynamics to a wind tunnel where the water is very shallow with restricted fetch.

The new model agrees well with the measurements other than the 2 outlier studies and is most similar to the SS80 model. The main difference in formulation between the new model and the SS80 model for water is the inclusion of the effects of whitecaps in enhancing deposition velocity. Since Equation 11 does not have any dependence on d_p the whitecaps effects are effectively a lower limit on V_d which raises the trough of the curve.

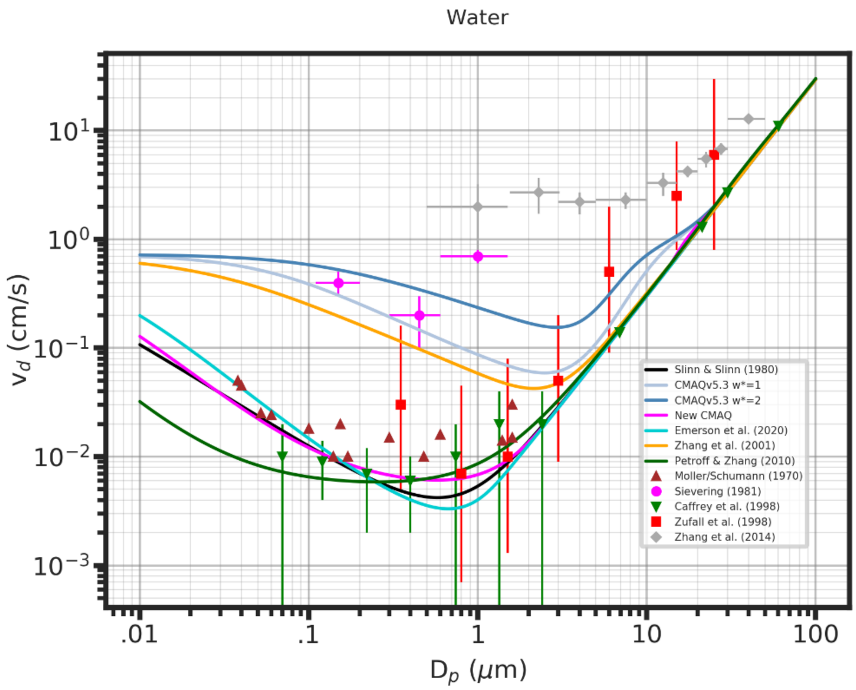

Figure 6. Same as Figure 2 but for water surfaces.

4.2 Discussion

Figure 7 shows the size dependence of the components of the dry deposition model for needleleaf forest. Clearly, the most effective component responsible for the S-shape curve for vegetated surfaces in the 0.2 – 10 μm range is the impaction on microscale features. The impaction collection efficiency acts as a threshold process where $E = 1$ where $St >$ ~3 for the formulation shown in Equation 7 and ramps down as St and d_p get smaller. The Stokes number, as represented by Equation 6, is a ratio of the inertial stopping distance of a particle to a characteristic length scale of an obstacle. For the macroscale term, which is common to nearly all current aerosol deposition models, the characteristic length represents the effects of the leaves. Figure 7 shows that the leaf scale impaction term has greatest effect on particles larger than about 5 μm. Note that for broadleaf forests the effects of this term are limited to even larger particles because the characteristic length scale is greater for broad leaves than for needle leaves.

The stopping distance for quasi-laminar sublayers on leaves can be estimated as $V_g\ u_*/g$. For u^* = 0.4 m/s the stopping distance decreases with decreasing d_p reaching 1 μm at d_p = 0.75 μm. A characteristic length of about 0.5 μm and a scaling factor f_{micro} of about 0.008 result in a good fit to the measured data as shown in Figure 2. A physical explanation of this process is that there exist microscale features on many leaves and stems that act as obstacles in the quasi-laminar sublayers. Many studies have shown increased deposition of $PM_{2.5}$ for broadleaf species that have dense hairs, ridges, grooves, or thick epicuticular wax layers as summarized above in Section 2. While needleleaf species generally don't have leaf hairs, they are often seen to be particularly efficient at $PM_{2.5}$ collection. A possible explanation is that the quasi-laminar sublayer grows from the leading edge of a surface and therefore will be thinner near the edge. Since the needle shape presents far more edge to the flow per area than broad leaves the deposition of sub-micron sized particles is more efficient. The hypothesis that more edge per area increases deposition is supported by the results of Zhang et al (2021) that showed increased $PM_{2.5}$ deposition to leaves with lower aspect ratio and greater fractal deviation. A physical interpretation of the scaling factor is that the edge effects of needle shaped leaves is only affecting a small portion of the leaf area. For broadleaf forest, the scaling factor accounts for the fraction of species that have dense leaf hairs or other microscale features and the sparsity of these features per leaf area.

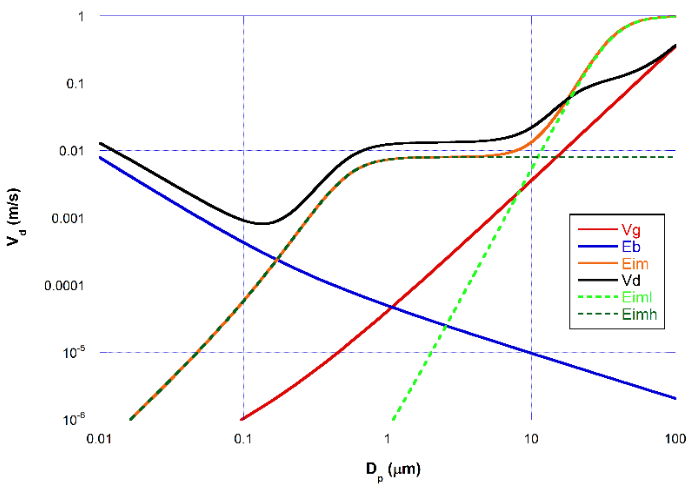

Figure 7. Size dependence of the components of the dry deposition model for needleleaf forest.

5. CMAQ implementation and evaluation

The new aerosol dry deposition model is implemented in the latest version of the CMAQ modeling system. The coupled version of the Weather Research and Forecasting (WRFv4.0.2) model and the CMAQv5.3 model are used to evaluate the new approach in air quality simulations over different-resolution domains for summer conditions in 2018.

5.1 Model implementation

Since CMAQ uses log-normal size distributions to represent Aitken, accumulation, and coarse modes, aerosol deposition velocities need to be integrated over the log-normal size distributions to calculate the 0^{th}, 2^{nd}, and 3^{rd} moments which represent the number, surface area, and volume of each mode, respectively. Therefore, the terms in the model that have explicit dependence on particle diameter *D* are integrated following Binkowski and Shankar (1995)

$$\hat{X}_k = \frac{1}{M_k}\int_{-\infty}^{\infty} XD^k(lnD)dlnD \text{ where } M_k = ND_g^k exp\left(\frac{k^2}{2}ln^2\sigma_g\right) \qquad (14)$$

where k is the moment (0,2,3) and *N* is the particle number concentration. The only terms in the new model that are explicit functions of particle diameter are Brownian diffusivity and gravitational settling velocity. For Brownian diffusivity the integrated form is,

$$\hat{D}_{Bk} = D_B(D_g)\left\{exp\left(\frac{(-2k+1)}{2}ln^2\sigma_g\right) + 1.246Kn_g exp\left(\frac{(-4k+4)}{2}ln^2\sigma_g\right)\right\} \qquad (15)$$

For gravitational settling velocity the integrated form is:

$$\hat{V}_{gk} = V_g\ (D_g)\left\{exp\left(\frac{(4k+4)}{2}ln^2\sigma_g\right) + 1.246Kn_g exp\left(\frac{(2k+1)}{2}ln^2\sigma_g\right)\right\} \qquad (16)$$

where D_g is the geometric mean diameter, σ_g is the geometric standard deviation, and the Knudsen number is $Kn_g = 2\lambda/D_g$ where λ is the mean free path. For the modal model, the dry deposition velocity is computed as described in Section 3 but with $\hat{D}_{Bk}$ and $\hat{V}_{gk}$ for k = 0,2,3 for the three moments of each of the three modes replacing D_B and V_g.

Figure 8 demonstrates the relationships among the dry deposition velocity moments for both the CMAQv5.3 model and the new model plotted against geometric mean diameter D_g compared to the non-integrated models vs particle diameter D_p applied for needleleaf forest. The 0th moment, which represents the number of the modal distribution, shows the effects of integration are to increase the $\hat{V}_d$ over the V_d for all sizes except in the plateau range (~1 - 3 μm) of the new model. The 3rd moment is similar to the 0th moment but with a shift to smaller D_g because the larger end of the distribution contributes more to volume than number.

Since the 3rd moment is proportional to mass, the 3rd moment of the dry deposition velocity represents the dry deposition velocity for mass concentration of aerosols. From Figure 8 it is evident that the mass deposition velocity for the new model is about an order of magnitude greater in the accumulation mode (D_g ~ 0.1 – 0.4 μm) than for the CMAQv5.3 model in forested areas. The effects of this increased dry deposition are assessed for CMAQ simulations across the conterminous US (CONUS) and at high resolution in the NE U.S.

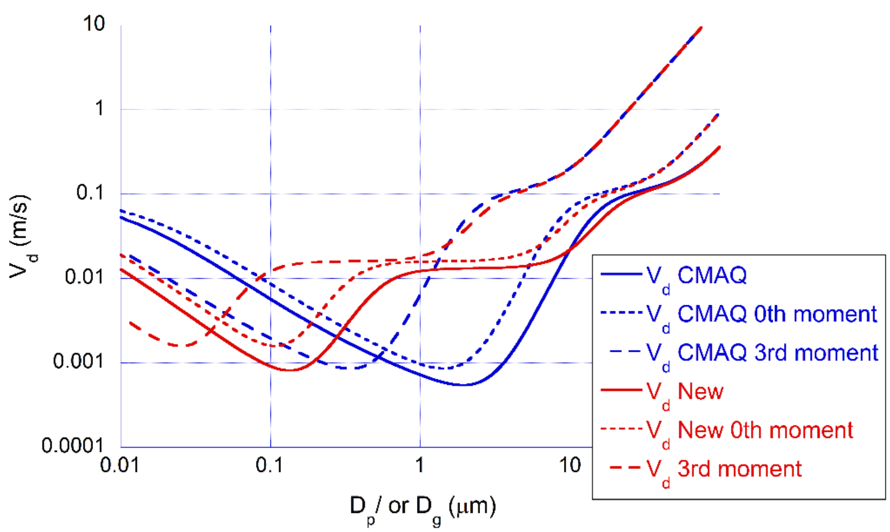

Figure 8. The dry deposition velocities for the 0th and 3rd moments of the CMAQv5.3 model and the new model compared to the non-integrated dry deposition velocities for

both models applied to needleleaf forest. The x-axis represents D_g for the $\hat{V}_d$ plots and D_p for the V_d plots.

5.2 WRF-CMAQ simulations

The coupled WRFv4.0.2/CMAQv5.3.1 model system was run in both the base configuration and with the new aerosol dry deposition model for several months in summer 2018. These simulations were based on modeling of the Long Island Sound Tropospheric Ozone Study (LISTOS) which was an intensive multi-institutional field study during the summer of 2018 (Karambelas 2020). The base model was run for three resolutions (12 km, 4 km, 1.33 km) where the outer domain covered the CONUS with one-way nested domains over the northeast (NE) states (4 km) and the New York/New Jersey/Connecticut (NY-NJ-CT) region (1.33 km). Detailed description of the model configuration and evaluation are presented by Torres-Vazquez et al. (2022). Model simulations using the new aerosol dry deposition model (NEW) were conducted for the 12 km CONUS domain for July 2018 and for the 1.33 km domain for July and August 2018. In both cases, identical simulations using the base CMAQv5.3 model (BASE) were also run. Initial conditions for the 12 km CONUS runs were from base case runs on June 21, 2018, that were started on January 1, 2018. The 1.33 km runs were initialized on July 1, 2018, from base case 1.33 km runs that started on May 2, 2018. All runs used the same boundary conditions and emissions as described by Torres-Vazquez et al. (2022).

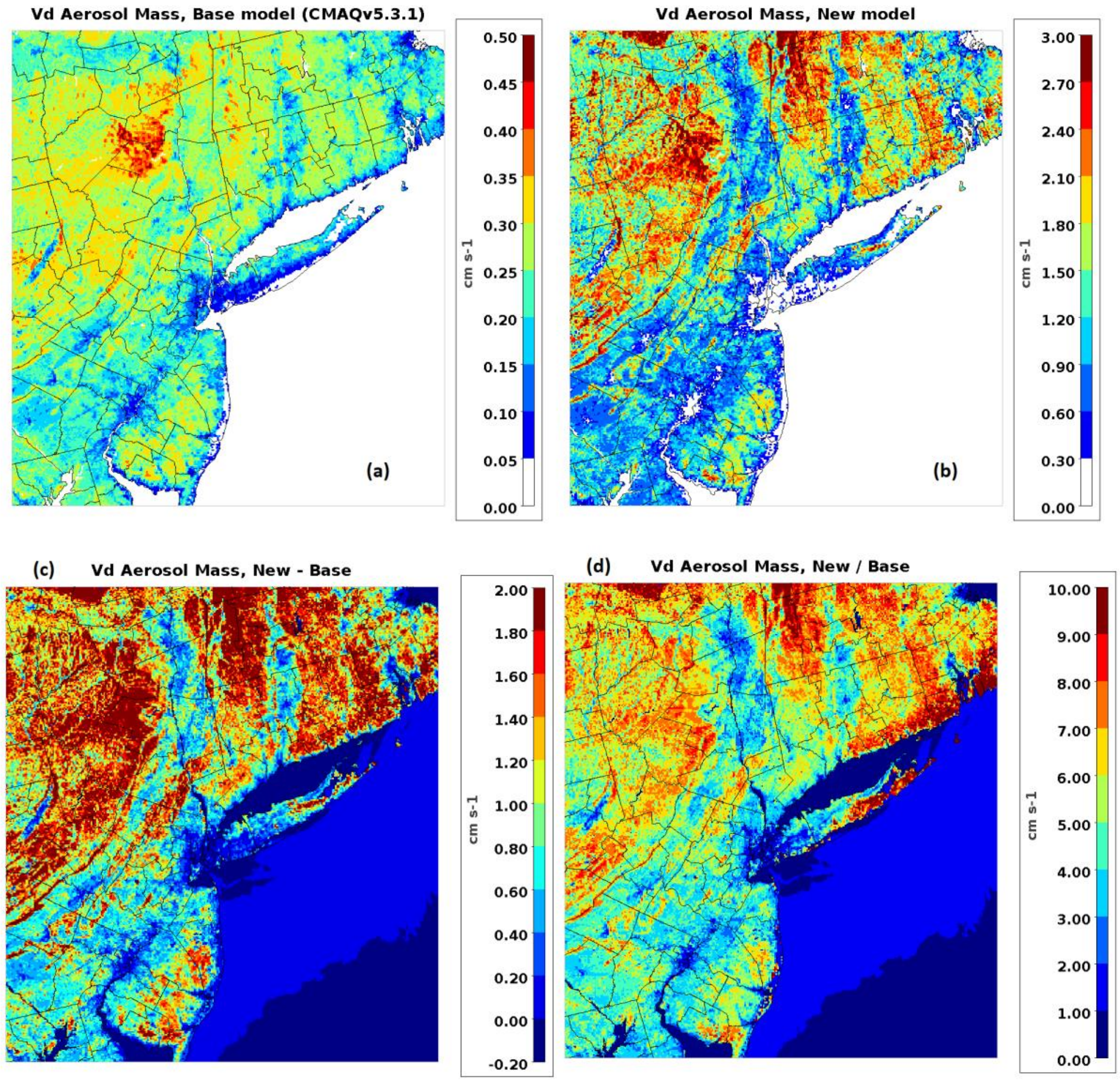

Figure 9. Accumulation mode mass dry deposition velocity from WRF-CMAQ on July 10, 2018 at 18 UTC (2 pm LT) for (a) BASE, (b) NEW, (c) NEW-BASE and (d) NEW/BASE over the New York/New Jersey/Connecticut 1.33-km domain. Note that the scales for (a) and (b) are different.

a) b)

Figure 9 shows the dry deposition velocity for accumulation mode mass on July 10, 2018, at 18 UTC (2 pm LT) for BASE, NEW, NEW-BASE and NEW/BASE over the NY-NJ-

CT 1.33 km resolution domain. July 10 was a particularly polluted day in the NYC area. Thus, it is an interesting case to study the effects of the new aerosol dry deposition model. The plots in Figure 9a and 9b both show how variations in land use strongly influence aerosol dry deposition for both BASE and NEW with greatest V_d in the forested areas. This is due to the combinations of large roughness length resulting in low aerodynamic resistance and large LAI. The greatest effects of the new model are indicated by the difference in the plot scales (BASE plots 0-0.5 cm/s; NEW plots 0-3.0 cm/s) which reflects an almost order of magnitude increase in V_d for accumulation mode mass in forested areas. Figures 9c and 9d, NEW – BASE and NEW/BASE, respectively, demonstrate that the largest differences are in the forested areas of Pennsylvania (PA), NY, Massachusetts (MA), CT, and Rhode Island (RI). The ratio of NEW/BASE (Figure 9d) is a factor of 8-10 in the heavily forested areas while it is only 1-3 in developed areas depending on the intensity of development. The inclusion of the building area as in Equation 12 increases V_d for accumulation mode mass in developed areas but only by a small amount as shown in Figure 10a. However, because the V_d in developed areas is small compared to vegetated areas, inclusion of the building effects has a substantial relative impact on the V_d (Figure 10b).

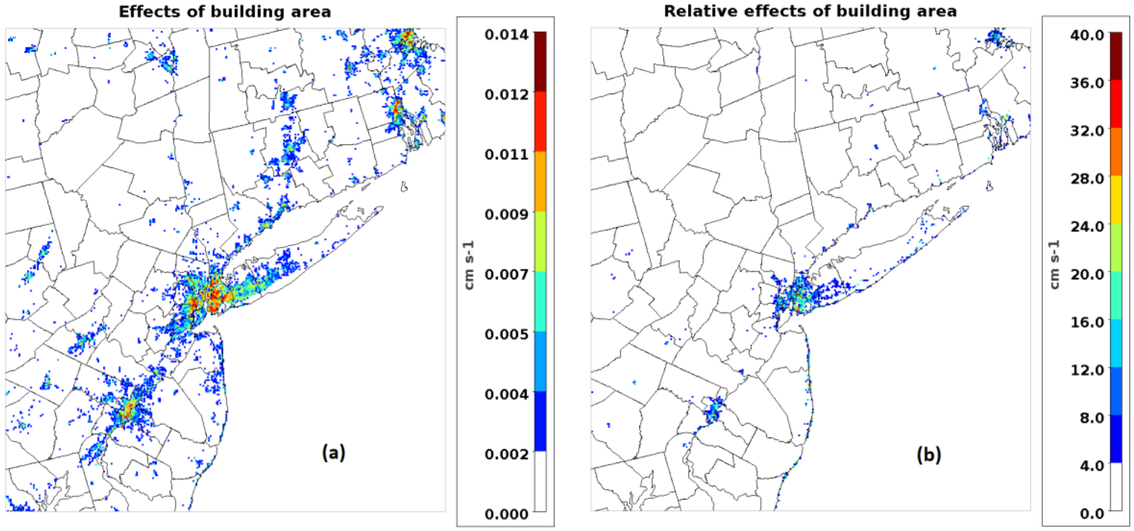

Figure 10. Difference (a) and relative difference (b) in V_d for accumulation mode mass between a NEW model run using *BAI* as in Equation 12 and a NEW mode run where *BAI* = 1 for July 10, 2018, at 18 UTC over the New York/New Jersey/Connecticut 1.33-km domain.

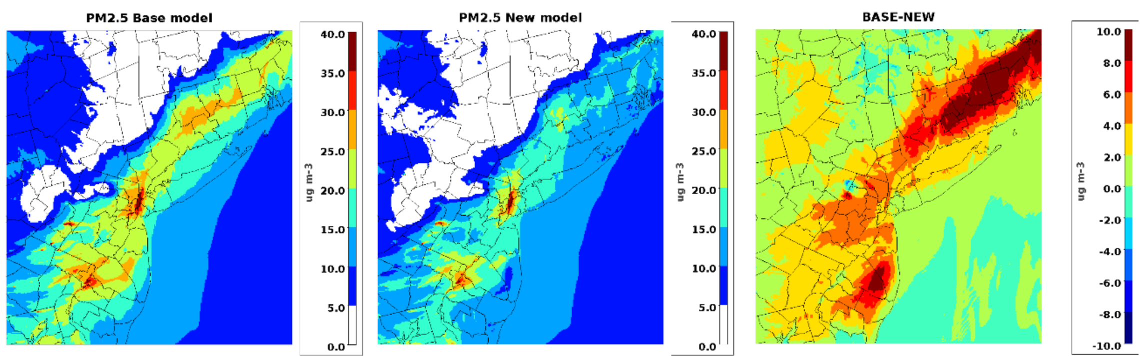

Figure 11. PM2.5 concentration on July 11, 2018, at 00 UTC (July 10, 8 pm LT) for BASE model (a) NEW model (b), and BASE - NEW (c) over the 1.33 km resolution domain.

Figure 11 shows the consequences of the new aerosol deposition velocities, shown in Figure 9, on $PM_{2.5}$ concentrations 6 hours later when the highest concentrations occurred in the region. The $PM_{2.5}$ concentrations at this time are greatest in the urban centers of NY city (NYC) and Philadelphia with high concentrations downwind to the northeast into CT and RI. The biggest effect of the new aerosol dry deposition is to substantially reduce the downwind concentrations in southern New England which is mostly forested. Another relative concentration maximum in the BASE model in southeastern NJ in an area known as the Pine Barrens, which is dense forest with a high fraction of needleleaf trees, is mostly absent in the NEW model run. Thus, the NEW model has larger effects on $PM_{2.5}$ concentrations in forested areas than other areas such as in urban areas. The peak concentrations in NYC only reduced by 10% while in some of the forested areas the NEW simulation reduces $PM_{2.5}$ concentration by more than 40%.

The afternoon (18 – 20 UTC) deposition velocity for accumulation mode mass was averaged for July 2018 for BASE and NEW model runs for the CONUS at 12 km resolution (Figure 12). Again, it is evident that the largest effects of the NEW model are in the forested areas mostly in the NE, western mountains and across the boreal forests of Canada. In some areas of the northeastern U.S. and southeastern Canada the NEW dry deposition velocities are 7-10 times the BASE values (Figure 12d). Note that Figure 12a shows some discontinuities at the Canadian border. This is due to the hybrid land use data that is a combination of higher resolution NLCD for the CONUS and the lower resolution Moderate Resolution Imaging Spectroradiometer (MODIS) land use data for elsewhere (Torres-Vazquez et al., 2022; Appel et al. 2014). In some of the sparsely vegetated areas in the west the difference between NEW and BASE is quite small while in the plains and predominately agricultural areas the difference is moderate.

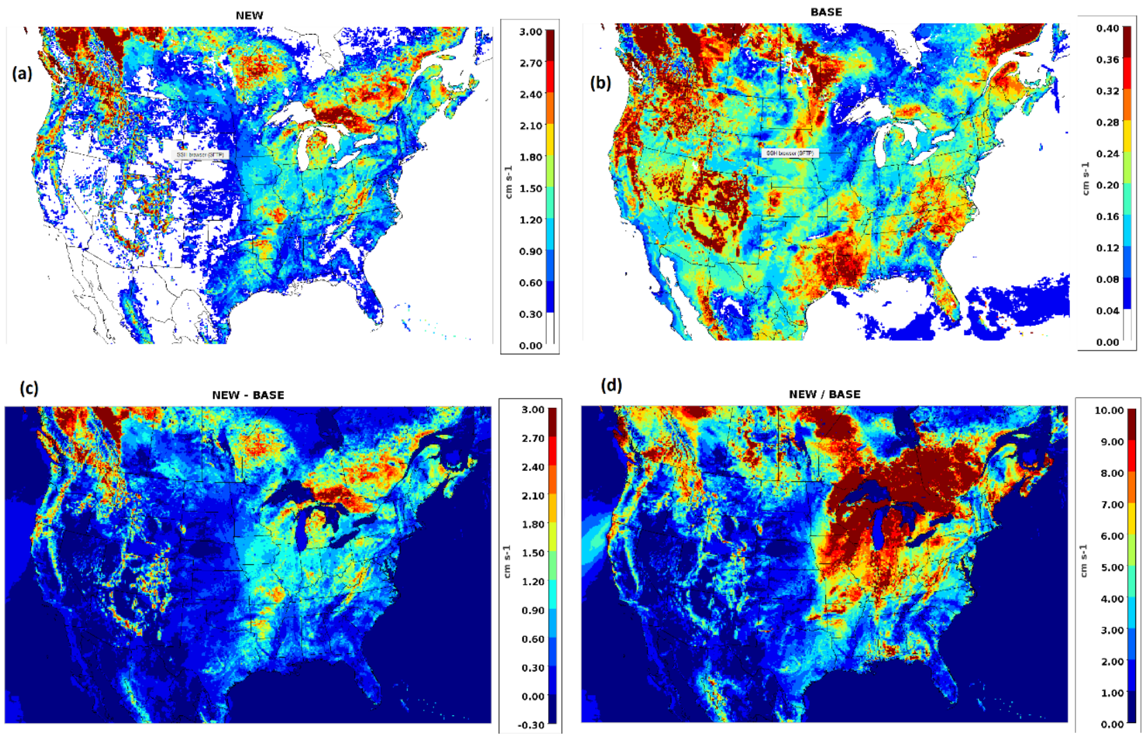

Figure 12. Afternoon (18 – 20 UTC) average accumulation mode mass dry deposition velocity for July 2018 on the CONUS 12 km domain for (a) BASE, (b) NEW, (c) NEW-BASE and (d) NEW/BASE. Note that the scales for (a) and (b) are different.

Increases in dry deposition velocity for accumulation mode aerosol using the NEW model increase the loading of aerosol species to land ecosystems. For example, Figure 13 shows that accumulated dry deposition mass of accumulation plus Aitken mode (approximately < 2.5 µm) ammonium aerosol for July 2018 is much greater for the NEW model than the BASE model. Thus, the NEW model has much greater predictions of nutrient loading of the aerosol components, especially to forested ecosystems. The NEW model increases deposition of other aerosol species as well that have may have health effects on livestock and wildlife. Predictions of exposure to hazardous chemicals, which may affect human health through ingestion of soil or contaminated produce, also increase with the NEW model.

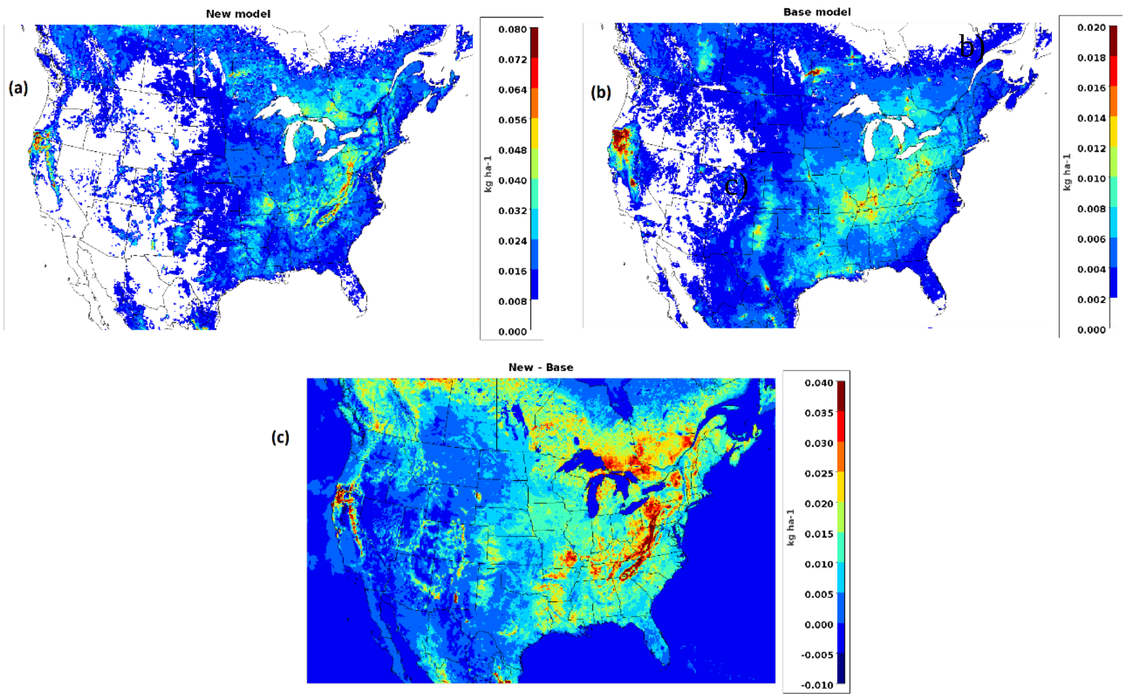

Figure 13. Accumulated dry deposition (kg/ha) over July 2018 of ammonium aerosol in accumulation plus Aitken modes. NEW model (a), BASE model (b) and NEW – BASE (c). Note that the scale for NEW model (a) is four times the scale for BASE model (b)

5.3 Simulation evaluation

The WRF-CMAQ simulations at both 1.33 km grid resolution in the NYC area and 12 km grid resolution for the CONUS were evaluated for $PM_{2.5}$ at the U.S. Environmental Protection Agency (EPA) Air Quality System (AQS) sites (AQS; http://www.epa.gov/aqs). Evaluations of model runs using the NEW aerosol dry deposition model were compared to the BASE model for summer season when the differences between NEW and BASE are greatest. Figure 14 shows diurnal bar charts for July and August 2018 for all AQS sites in the 1.33 km grid resolution domain (see figure 9 for size of domain) and for July 2018 at AQS sites in the 12 km grid resolution CONUS domain. The colored bars represent the 25th and 75th percentiles of the $PM_{2.5}$ concentration distributions for NEW, BASE, and AQS. The black line in each bar indicates the median value. For the fine grid NE domain both NEW and BASE are high compared to AQS for every hour but NEW is closer to AQS. The diurnal pattern of the modeled concentrations is different from the observation with the greatest concentrations around 6 am and lowest in late afternoon at about 17 LT while the AQS concentrations show very little diurnal variation. This diurnal pattern is typical for modeled concentrations of species with a large ground emitted fraction (i.e., NOx, CO, and $PM_{2.5}$). This is a known issue that is related to the suppressed vertical mixing at night and the much greater mixing during the day. The near dawn peak results from the combination of suppressed mixing and high emissions during the morning rush hour. Note that this issue has been improved in recent years through updates to the PBL scheme in the WRF-CMAQ system (e.g., Toro et al., 2021). Another contributing factor is the uncertainty in emissions and especially the hourly attribution of emissions.

Evaluation of the 12 km CONUS simulations shows similar diurnal pattern with peak concentrations around sunrise and lowest concentrations in afternoon (EDT). The AQS concentrations are more constant over the day than the models but with a slight variation with a similar diurnal pattern. The BASE model is again higher than the observations for every hour, but the NEW model is slightly high during the night and slightly low during the day.

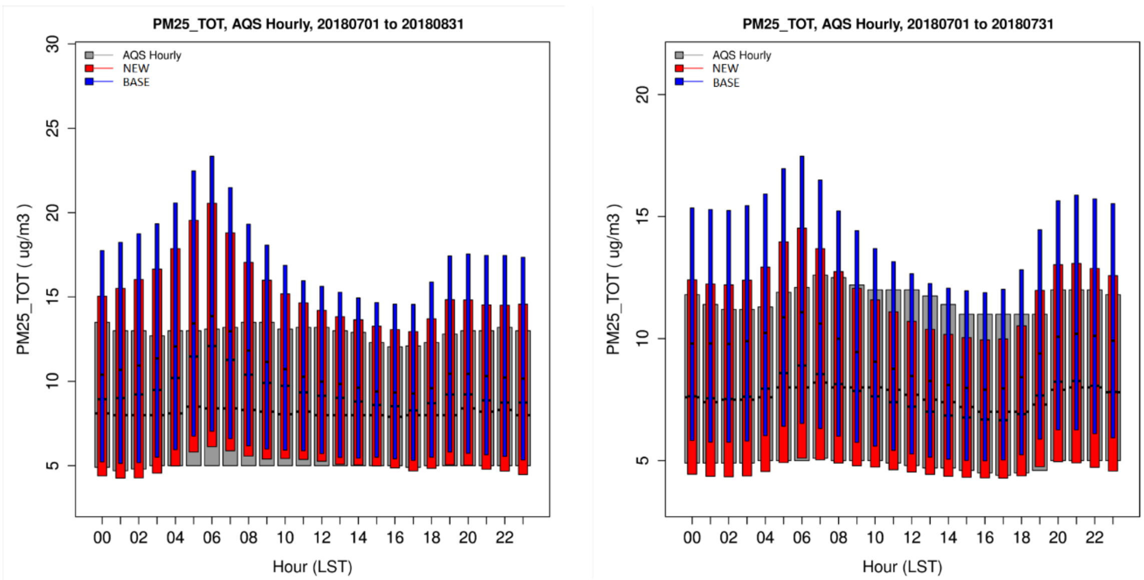

Figure 14. Hourly bar plots of PM2.5 aggregated over July and August 2018 for the northeast 1.33 km domain on left and over July 2018 for the 12 km CONUS on right. The colored bars represent the 25th and 75th percentiles of the $PM_{2.5}$ concentration distributions for NEW (red), BASE (blue), and AQS observations (grey).

Spatial evaluation of $PM_{2.5}$ in the 1.33 km domain for NEW and BASE are shown in Figure 15. For both NEW and BASE the average bias is greatest in NYC where high emissions are concentrated in small grid cells. The BASE (15b) also has high bias at most other sites. The NEW (15a) has less high bias and is roughly even between slightly high and slightly low biases outside of NYC. The lower plots show reduced bias (15d) and mean error (15c) for NEW compared to BASE at 83% and 93% of the AQS sites, respectively. The urban effects of building area reduce the high bias in the cities but only by a very small amount (less than 0.3%; not shown).

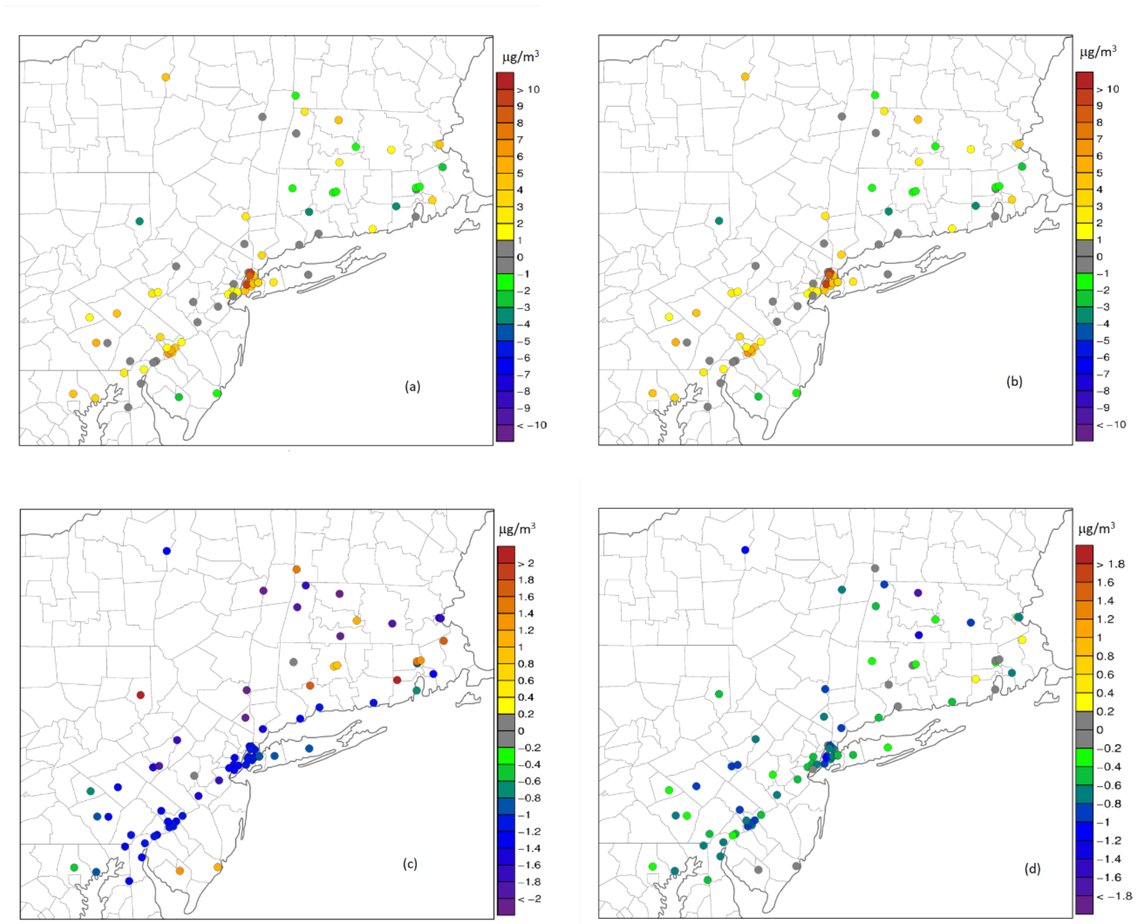

Figure 15. Evaluation of modeled hourly $PM_{2.5}$ compared to AQS measurements averaged for July and August 2018: (a) NEW model bias, (b) BASE model bias, (c) NEW – BASE absolute bias difference, and (d) NEW – BASE mean absolute error difference.

Similar spatial evaluation for the 12 km CONUS simulations is shown in Figure 16. Overall, the $PM_{2.5}$ bias averaged over July 2018 at AQS sites is reduced at 64% of the sites and the mean error is reduced at 77% of the sites. In areas where the BASE $PM_{2.5}$ concentrations are biased high such as the Great Lakes region, most of the sites in the east, and the west coast, the NEW model reduces bias and error. In areas where the BASE model was low, such as Texas and the southern plains, the bias is slightly increased although mean absolute error is less affected. In these areas the difference in dry deposition velocity is relatively small because there is less vegetation and not much forest. Note that the increased bias and error at some sites in SW Oregon and northern CA are related to very high $PM_{2.5}$ concentrations caused by wildfires.

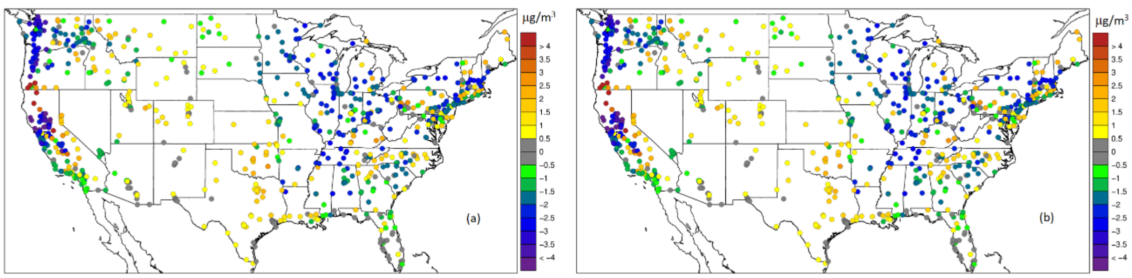

Figure 16. Evaluation of modeled hourly $PM_{2.5}$ compared to AQS measurements averaged for July 2018: (a) NEW – BASE absolute bias difference, and (b) NEW – BASE mean absolute error difference.

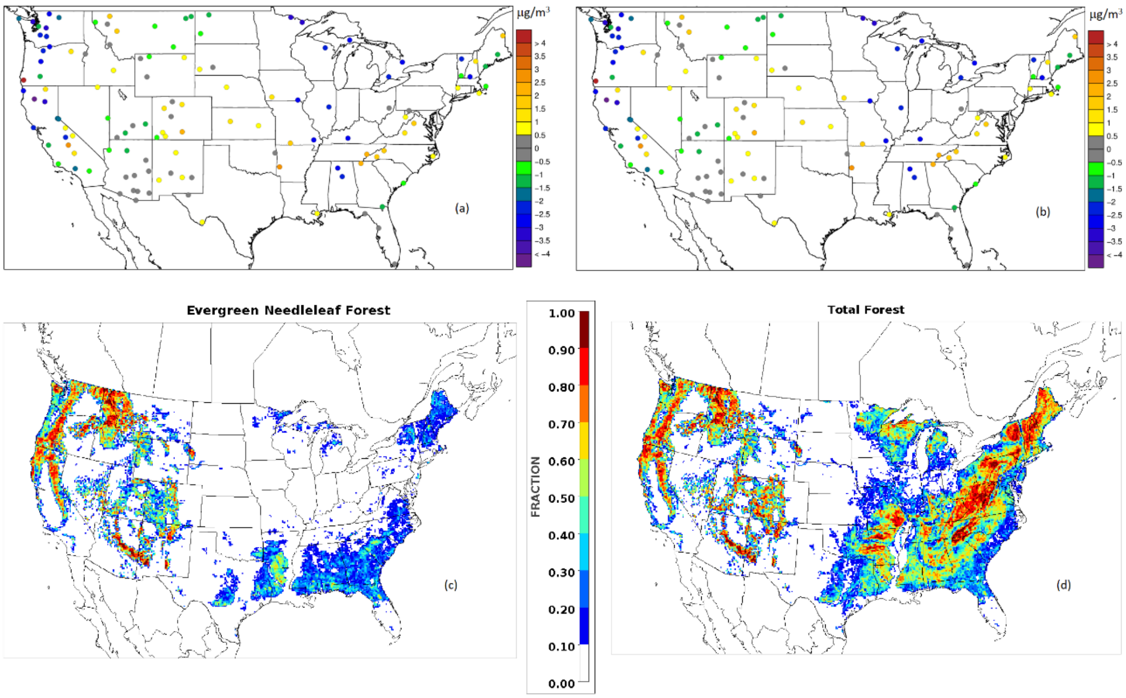

Figure 17. Evaluation of modeled hourly $PM_{2.5}$ compared to IMPROVE measurements averaged for July 2018: (a) NEW – BASE absolute bias difference, (b) NEW – BASE mean absolute error difference, (c) gridded evergreen needleleaf forest fraction, (d) total gridded forest fraction.

Figure 17 shows $PM_{2.5}$ bias and error averaged over July 2018 at IMPROVE sites (the Interagency Monitoring of PROtected Visual Environments (IMPROVE; http://vista.cira.colostate.edu/Improve/). Since the IMPROVE network highlights Class I areas, many of the sites are in forested regions, particularly in the Pacific NW. Figure 17c shows that many sites in WA, OR and northern CA are in evergreen needleleaf forest and that many of these sites have the greatest reduction in bias and error of $PM_{2.5}$.

6. Conclusions and future work

The modeling of dry deposition in general, and aerosol dry deposition in particular, contribute large amounts of uncertainty to air quality and climate models (e.g., Solazzo et al., 2012; Mahowald et al., 2017). Thus, improving the mechanistic underpinnings of dry deposition calculations helps improve accuracy of the modeling systems. The new development to the aerosol dry deposition model was driven by the aggregation of experimental data showing that existing models are unable to accurately replicate the observed relationship between particle size and dry deposition velocity especially for forested areas. Since the quasi-laminar sublayer resistance R_b is usually the controlling resistance during peak deposition conditions (daytime), the new developments focus on revision of the R_b parameterizations, particularly the impaction efficiency. The development process was to revise the impaction efficiency to get better agreement with the aggregate measurements while maintaining physically plausible rationales. The key innovation was to add a second term to the impaction efficiency (equation 7) that represents impaction on microscale obstacles. For broadleaf vegetation the concept is that many species have leaf hairs or other microscale roughness features. However, needleleaf species generally do not have hairs but they may have ridges or other microscale obstacles. Since experimental studies have found that needleleaf species have high aerosol deposition rates, it is theorized that the needle shape itself may be a key factor as discussed in section 5.

The main impact of the new model is to increase dry deposition velocity in the accumulation size range. This has a large effect on $PM_{2.5}$ especially in forested areas where the dry deposition velocity of accumulation mode mass can increase up to an order of magnitude compared to the current model in CMAQv5.3. For the high-resolution model application to the LISTOS the new model reduced $PM_{2.5}$ concentration up to 40% downwind of NYC in CT for the case shown in Figure 11. For these applications in summer of 2018 where the BASE model generally overestimates $PM_{2.5}$, the NEW model which has much greater accumulation mode mass dry deposition, results in mostly better agreement with observations. However, aerosol concentrations are very difficult to model accurately not just because of uncertainties in dry deposition but also uncertainties in emissions, transport and diffusion, wet scavenging, and very complex chemistry which involves semi-volatile organic and inorganic species (Appel et al., 2021).

Continued research on aerosol dry deposition is needed. More field studies, especially for some of the lesser studied vegetation land use types such as croplands, grasslands, and broadleaf deciduous forests, would help to confirm or refute the new model paradigm for different vegetation types and help define parameters such as the macro and micro scale characteristic obstacle dimensions and scaling factors. In addition to comparisons to aggregates of measurements we also plan to model individual field studies in detail where the aerosol dry deposition model is driven by observed micrometeorology and canopy characteristics on an observational timestep basis (30 min or 1 hour).

Another next step in this research is to include the effects of brown vegetation in the model. Currently, the vegetation fraction and LAI are specified in the WRF-CMAQ system either by land-use category look-up table, where the parameters seasonally vary between minimum and maximum values, or from MODIS satellite fraction of absorbed photosynthetically active radiation (FPAR) and LAI retrievals. In either case, the vegetation parameters are meant to represent live vegetation for evapotranspiration and stomatal uptake of gaseous pollutants. However, for aerosol deposition, brown vegetation can also provide surfaces for deposition. Therefore, we are planning to include MODIS non-photosynthetic vegetation (NPV) and photosynthetic vegetation (PV) fractions in the aerosol dry deposition model. Preliminary tests show that the inclusion of NPV increases aerosol deposition over large areas of the western US. Implementation of NPV has already been included for windblown dust emissions where NPV reduces dust emissions by shielding the soil surface from the wind (Huang and Foroutan 2021).

Disclaimer

Although this work was reviewed by EPA and approved for publication, it may not necessarily reflect official Agency policy. Mention of commercial products does not constitute endorsement by the Agency.

Acknowledgments

We gratefully acknowledge the free availability and use of observational data sets from EPA AQS (available at https://www.epa.gov/aqs) and the IMPROVE network (available at http://vista.cira.colostate.edu/Improve). . We thank Christian Hogrefe and Chris Nolte for comments and suggestions on the initial version of this paper.

Data Availability Statement

Data used to generate figures and table are available at https://doi.org/10.23719/1524715.

References

Ahlm, L., Krejci, R., Nilsson, E. D., Martensson, E. M., Vogt, M. and co-authors. 2010. Emission and dry deposition of accumulation mode particles in the Amazon Basin. Atmos. Chem. Phys. 10, 10237–10253. doi:10.5194/acp-10-10237-2010.

Albert, M. F., Anguelova, M. D., Manders, A. M., Schaap, M., & Leeuw, G. D. (2016). Parameterization of oceanic whitecap fraction based on satellite observations. *Atmospheric Chemistry and Physics*, **16**(21), pp.13725-13751.

Allen, A. G., Harrison, R. M. and Nicholson, K. W. 1991. Dry deposition of fine aerosol to a short grass surface. Atmos. Environ. 25A, 2671–2676.

Appel, K. W., Bash, J. O., Fahey, K. M., Foley, K. M., Gilliam, R. C., Hogrefe, C., Hutzell, W. T., Kang, D., Mathur, R., Murphy, B. N., Napelenok, S. L., Nolte, C. G., Pleim, J. E., Pouliot, G. A., Pye, H. O. T., Ran, L., Roselle, S. J., Sarwar, G., Schwede, D. B., Sidi, F. I., Spero, T. L., and Wong, D. C.: The Community Multiscale Air Quality (CMAQ) model versions 5.3 and 5.3.1: system updates and evaluation, Geosci. Model Dev., 14, 2867–2897, https://doi.org/10.5194/gmd-14-2867-2021, 2021.

Appel, K. W., Gilliam, R. C., Pleim, J. E., Pouliot, G. A., Wong, D. C., Hogrefe, C., et al. 598 (2014). Improvements to the WRF-CMAQ modeling system for fine-scale air quality 599 simulations. EM: Air and Waste Management Association's Magazine for Environmental 600 Managers (September).

Beckett, K.P., Freer-Smith, P.H. and Taylor, G., 2000. Particulate pollution capture by urban trees: effect of species and windspeed. Global change biology, 6(8), pp.995-1003.

Beswick, K. M., Hargreaves, K. J., Gallagher, M. W., Choularton, T. W. and Fowler, D. 1991. Size-resolved measurements of cloud droplet deposition velocity to a forest canopy using an eddy correlation technique. Q. J. R. Met. Soc. 117, 623–645. doi:10.1002/qj.49711749910.

Bey, I., D. J. Jacob, R. M. Yantosca, J. A. Logan, B. Field, A. M. Fiore, Q. Li, H. Liu, L. J. Mickley, and M. Schultz, Global modeling of tropospheric chemistry with assimilated meteorology: Model description and evaluation, J. Geophys. Res., 106, 23,073-23,096, 2001.

Binkowski, F. S. & Shankar, U. (1995). The regional particulate matter model: 1. Model description and preliminary results. *Journal of Geophysical Research: Atmospheres*, **100**(D12), pp.26191-26209.

Buzorius, G., Rannik, U., Makela, J. M., Keronen, P., Vesala, T. and co-authors. 2000. Vertical aerosol fluxes measured by the eddy covariance method and deposition of nucleation mode particles above a Scots pine forest in southern Finland. J. Geophys. Res. 105, 19905–19916.

Byun, D., & Schere, K. L. (2006). Review of the governing equations, computational algorithms, and other components of the models-3 Community Multiscale Air Quality (CMAQ) modeling system. Applied Mechanics Reviews, 59(1–6). https://doi.org/10.1115/1.2128636

Caffrey, P. F., Ondov, J. M., Zufall, M. J. and Davidson, C. I. 1998. Determination of size-dependent dry particle deposition velocities with multiple intrinsic elemental tracers. Environ. Sci. Technol. 32, 1615–1622. doi:10.1021/es970644f.

Chamberlain, A. C. 1967. Transport of Lycopodium spores and other small particles to rough surfaces. Proceedings of the Royal Society of London 296A, 45–70.

Chen, L., Liu, C., Zhang, L., Zou, R., & Zhang, Z. (2017). Variation in tree species ability to capture and retain airborne fine particulate matter (PM 2.5). *Scientific Reports*, **7**(1), pp.1-11.

Chiam, Z., Song, X. P., Lai, H. R., & Tan, H. T. W. (2019). Particulate matter mitigation via plants:Understanding complex relationships with leaf traits. *Science of the total environment*, **688**, pp.398-408

Clough, W. S. 1975. The deposition of particles on moss and grass surfaces. Atmos. Environ. 9, 1113–1119. doi:10.1016/0004-6981(75)90187-0.

Connan O, Pellerin G, Maro D, Damay P, Hébert D, et al. 2018. Dry deposition velocities of particles on grass: field experimental data and comparison with models. J. Aerosol Sci. 126:58–67

Cunningham, E., 1910. On the velocity of steady fall of spherical particles through fluid medium. Proc. Roy. Soc. A 83, 357.

Deventer, M.J., Held, A., El-Madany, T.S. and Klemm, O., 2015. Size-resolved eddy covariance fluxes of nucleation to accumulation mode aerosol particles over a coniferous forest. Agricultural and Forest Meteorology, 214, pp.328-340.

Emerson, E. W., Hodshire, A. L., DeBolt, H. M., Bilsback, K. R., Pierce, J. R., McMeeking, G. R., & Farmer, D. K. (2020). Revisiting particle dry deposition and its role in radiative effect estimates. *Proceedings of the National Academy of Sciences*, **117**(42), pp.26076-26082.

ENVIRON. 2020. User's Guide, Comprehensive Air Quality Model with Extensions (CAMx), Version 7.10. https://camx-wp.azurewebsites.net/Files/CAMxUsersGuide_v7.10.pdf.

Farmer, D. K., Boedicker, E. K., & DeBolt, H. M. (2021). Dry Deposition of Atmospheric Aerosols: Approaches, Observations, and Mechanisms. *Annual Review of Physical Chemistry*, **72**, pp.375-397.

Gallagher, M. W., Choularton, T. W., Morse, A. P. and Fowler, D. 1988. Measurements of the size dependence of cloud droplet deposition at a hill site. Q. J. R. Meteorol. Soc. 114, 1291–1303.

Gallagher, M. W., Beswick, K. M., Duyzer, J., Westrate, H., Choularton, T. W. and co-authors. 1997. Measurements of aerosol fluxes to Speulder Forest using a micrometeorological technique. Atmos. Environ. 31, 359–373.

Gaman, A., Rannik, U., Aalto, P., Pohja, T., Siivola, E. and coauthors. 2004. Relaxed eddy accumulation system for size resolved aerosol particle flux measurements. J. Atmos. Oceanic Technol. 21, 933–943.

Gong, W., Dastoor, A.P., Bouchet, V.S., Gong, S., Makar, P.A., Moran, M.D., Pabla, B., Ménard, S., Crevier, L.P., Cousineau, S. and Venkatesh, S., 2006. Cloud processing of gases and aerosols in a regional air quality model (AURAMS). Atmospheric Research, 82(1-2), pp.248-275.

Gong, W., Makar, P.A., Zhang, J., Milbrandt, J., Gravel, S., Hayden, K.L., Macdonald, A.M. and Leaitch, W.R., 2015. Modelling aerosol–cloud–meteorology interaction: A case study with a fully coupled air quality model (GEM-MACH). Atmospheric Environment, 115, pp.695-715.

Gordon, M., Staebler, R. M., Liggio, J., Vlasenko, A., Li, S.-M. and co-authors. 2011. Aerosol flux measurements above a mixed forest at Borden, Ontario. Atmos. Chem. Phys. 11, 6773–6786.

Grönholm, T., Aalto, P. P., Hiltunen, V., Rannik, U., Rinne, J. and co-authors. 2007. Measurements of aerosol particle dry deposition velocity using the relaxed eddy accumulation technique. Tellus 59B, 381–386.

Grönholm, T., Launiainen, S., Ahlm, L., Martensson, E. M., Kulmala, M. and co-authors. 2009. Aerosol particle dry deposition to canopy and forest floor measured by two-layer eddy covariance system. J. Geophys. Res. 114, D04202. doi:1029/2008JD010663.

Grosch, S. and Schmitt, G. 1988. Experimental Investigations on the Deposition of Trace Elements in Forest Area. In: Environmental Meteorology (eds. K. Grefen and L. Lobel). Kluwer Academic Publishers, Dordrecht, The Netherlands, pp. 201–216.

Hicks, B. B., Wesely, M. L., Durham, J. L. and Brown, M. A. 1982. Some direct measurements of atmospheric sulfur fluxes over a pine plantation. Atmos. Environ. 16, 2899–2903.

Hicks, B. B., Matt, D. R., McMillen, R. T., Womack, J. D., Wesely, M. L. and co-authors. 1989. A field investigation of sulfate fluxes to a deciduous forest. J. Geophys. Res. 94, 13003–13011.

Hofken, K. D. and Gravenhorst, G. 1982. Deposition of atmospheric aerosol particles to beech- and spruce forest. In: Deposition of Atmospheric Pollutants (eds. H. W. Georggi and J. Pankrath). D. Reidel Publishing Company, Oberursel/Taunus, Germany, pp. 191–194.

Huang, X. and Foroutan, H., 2021. Effects of Non-Photosynthetic Vegetation on Dust Emissions. Earth and Space Science Open Archive ESSOAr.

Hummelshøj, P. N. O. S. E., Jensen, N. O., & Larsen, S. E. (1992). Particle dry deposition to a sea surface. Precipitation scavenging and atmosphere-surface exchange, *Hemisphere Publishing Corporation*, *Washington*, **5562**, pp.829-840.

Hummelshøj, P. 1994. Dry Deposition of Particles and Gases. PhD Thesis, Technical University of Denmark.

IPCC, 2021: Climate Change 2021: The Physical Science Basis. Contribution of Working Group I to the Sixth Assessment Report of the Intergovernmental Panel on Climate Change [Masson-Delmotte, V., P. Zhai, A. Pirani, S.L. Connors, C. Péan, S. Berger, N. Caud, Y. Chen, L. Goldfarb, M.I. Gomis, M. Huang, K. Leitzell, E. Lonnoy, J.B.R. Matthews, T.K. Maycock, T. Waterfield, O. Yelekçi, R. Yu, and B. Zhou (eds.)]. Cambridge University Press. In Press.

Karambelas, A., LISTOS: Toward a Better Understanding of New York City's Ozone Pollution Problem, EM, October 2020.

Lavi, A., Farmer, D. K., Segre, E., Moise, T., Rotenberg, E. and co-authors. 2013. Fluxes of fine particles over a semi-arid pine forest: Possible effects of a complex terrain. Aerosol. Sci. Technol. 47, 906–915.

Leonard, R.J., McArthur, C. and Hochuli, D.F., 2016. Particulate matter deposition on roadside plants and the importance of leaf trait combinations. Urban Forestry & Urban Greening, 20, pp.249-253.

Lorenz, R. and Murphy, C. E. Jr. 1989. Dry deposition of particles to a pine plantation. Boundary-Layer Meteorol. 46, 355–366.

Mahowald, N.M., Scanza, R., Brahney, J. et al. Aerosol Deposition Impacts on Land and Ocean Carbon Cycles. Curr Clim Change Rep 3, 16–31 (2017). https://doi.org/10.1007/s40641-017-0056-z

Mammarella, I., Rannik, U., Aalto, P., Keronen, P., Vesala, T. and co-authors. 2011. Long-term aerosol particle flux observations. Part II: Particle size statistics and deposition velocities. Atmos. Environ. 45, 3794–3805.

Matsuda, K., Watanabe, I., Mizukami, K., Ban, S. and Takahashi, A. 2015. Dry deposition of PM2.5 sulfate above a hilly forest using relaxed eddy accumulation. Atmos. Environ. 107, 255–261.

Moller, U. and Schumann, G. 1970. Mechanisms of transport from the atmosphere to the Earth's surface. J. Geophys. Res. 75, 3013–3019.

Nemitz, E., Gallagher, M. W., Duyzer, J. H. and Fowler, D. 2002. Micrometeorological measurements of particle deposition velocities to moorland vegetation. Q. J. R. Meteorol. Soc. 128, 2281–2300.

Neumann, H. H. and den Hartog, G. 1985. Eddy correlation measurements of atmospheric fluxes of ozone, sulphur, and particulates during the Champaign Intercomparison Study. J. Geophys. Res. 90, 2097–2110.

Ould-Dada, Z. 2002. Dry deposition profile of small particles within a model spruce canopy. Sci. Total Environ. 286, 83–96.

Pleim, J. and Ran, L. 2011. Surface flux modeling for air quality applications. Atmosphere 2, 271–302.

Perini, K., Ottelé, M., Giulini, S., Magliocco, A. and Roccotiello, E., 2017. Quantification of fine dust deposition on different plant species in a vertical greening system. Ecological engineering, 100, pp.268-276.

Petroff, A. and Zhang, L. 2010. Development and validation of a size-resolved particle dry deposition scheme for application in aerosol transport models. Geosci. Model Dev. 3, 753–769.

Petroff, A., Murphy, J.G., Thomas, S.C. and Geddes, J.A., 2018. Size-resolved aerosol fluxes above a temperate broadleaf forest. Atmospheric Environment, 190, pp.359-375.

Pryor, S. C., Barthelmie, R. J., Geernaert, L. L. S., Ellermann, T., & Perry, K. D. (1999). Speciated particle dry deposition to the sea surface: results from ASEPS'97. *Atmospheric Environment*, **33**(13), pp.2045-2058.

Pryor, S. C. 2006. Size-resolved particle deposition velocities of sub-100nm diameter particles over a forest. Atmos. Environ. 40, 6192–6200.

Pryor, S.C., Larsen, S.E., Sørensen, L.L., Barthelmie, R.J., Grönholm, T. and co-authors. 2007. Particle fluxes over forests: analyses of flux methods and functional dependencies. J. Geophys. Res.: Atmos., 112, D07205, doi:10.1029/2006JD008066.

Pryor, S.C., Gallagher, M., Sievering, H., Larsen, S.E., Barthelmie, R.J., Birsan, F., Nemitz, E., Rinne, J., Kulmala, M., Grönholm, T. and Taipale, R., 2008. A review of measurement and modelling results of particle atmosphere–surface exchange. Tellus B: Chemical and Physical Meteorology, 60(1), pp.42-75.

Pryor, S. C., Barthelmie, R. J., Spaulding, A. M., Larsen, S. E., and Petroff, A. (2009). Size-Resolved Aerosol Particle Fluxes over Forests. J. Geophys. Res., 114, doi:10.1029/2009JD012248.

Sæbø, A., Popek, R., Nawrot, B., Hanslin, H.M., Gawronska, H., Gawronski, S.W., 2012. Plant species differences in particulate matter accumulation on leaf surfaces. Sci. Total Environ. 427 (-428), 347–354, http://dx.doi.org/10.1016/j.scitotenv.2012.03.084.

Saylor, R. D., Baker, B. D., Lee, P., Tong, D., Pan, L., & Hicks, B. B. (2019). The particle dry deposition component of total deposition from air quality models: right, wrong or uncertain?. *Tellus B: Chemical and Physical Meteorology*, **71**(1), p.1550324.

Sievering, H. 1981. Profile measurements of particle mass transfer at the air-water interface. Atmos. Environ. 15, 123–129.

Sievering, H. 1982. Profile measurements of particle dry deposition velocity at an air-land interface. Atmos. Environ. 16, 301–306.

Sievering, H. 1988. Small-particle dry deposition measurements: A comparison of gradient and eddy flux techniques over agricultural fields, In: Annual Meeting of Air Pollution Control Association, Dallas, Texas, June 19–24, 6, pp. 88–101.

Slinn, W. G. N. 1977. Some approximations for the wet and dry removal of particles and gases from the atmosphere. Water Air Soil Pollut. 7, 513–543.

Slinn, S. A. & Slinn, W. G. N. (1980). Predictions for particle deposition on natural waters. *Atmospheric Environment (1967)*, **14**(9), pp.1013-1016.

Slinn, W. G. N. (1982). Predictions for particle deposition to vegetative canopies. *Atmospheric Environment (1967)*, **16**(7), pp.1785-1794.

Solazzo, E., Bianconi, R., Pirovano, G., Matthias, V., Vautard, R., Moran, M.D., Appel, K.W., Bessagnet, B., Brandt, J., Christensen, J.H. and Chemel, C., 2012. Operational model evaluation for particulate matter in Europe and North America in the context of AQMEII. *Atmospheric environment*, **53**, pp.75-92.

Stokes, G. G. 1851. On the effect of internal friction of fluids on the motion of pendulums. Transactions of the Cambridge Philosophical Society. 9, part ii: 8–106.

Sun, F., Yin, Z., Lun, X., Zhao, Y., Li, R. and co-authors. 2014. Deposition velocity of PM2.5 in the winter and spring above deciduous and coniferous forests in Beijing, China. PLoS One 9, e97723. doi: 10.1371/journal.pone.0097723.

Torres-Vazquez, A., Pleim, J., Gilliam, R., Pouliot, G., 2022, Performance Evaluation of the Meteorology and Air Quality Conditions from 1 Multiscale WRF CMAQ Simulations for the Long Island Sound Tropospheric 2 Ozone Study (LISTOS), submitted to Journal of Geophysical Research: Atmospheres

Toro, C., Foley, K., Simon, H., Henderson, B., Baker, K.R., Eyth, A., Timin, B., Appel, W., Luecken, D., Beardsley, M. and Sonntag, D., 2021. Evaluation of 15 years of modeled atmospheric oxidized nitrogen compounds across the contiguous United States. Elem Sci Anth, 9(1), p.00158.

Venkatram, A. and Pleim, J. 1999. The electrical analogy does not apply to modeling dry deposition of particles. Atmos. Environ. 33, 3075–3076.

Vong, R. J., Vong, I. J., Vickers, D. and Covert, D. S. 2010. Size-dependent aerosol deposition velocities during BEARPEX'07. Atmos. Chem. Phys. 10, 5749–5758.

Vong, R. J., Vickers, D. and Covert, D. S. 2004. Eddy correlation measurements of aerosol deposition to grass. Tellus 56B, 105–117.

Waraghai, A. and Gravenhorst, G. 1989. Dry deposition of atmospheric particles to an old spruce stand, in: Mechanisms and Effects of Pollutant Transfer into Forests. (ed. H. W. Georgii), Kluwer Academic Publishers, London, pp. 77–86.

Weerakkody, U., Dover, J. W., Mitchell, P., & Reiling, K. (2018). Evaluating the impact of individual leaf traits on atmospheric particulate matter accumulation using natural and synthetic leaves. *Urban forestry & urban greening*, **30**, pp.98-107.

Wesely, M. L., Hicks, B. B., Dannevik, W. P., Frisella, S. and Husar, R. B. 1977. An eddy-correlation measurement of particulate deposition from the atmosphere. Atmos. Environ. 11, 561–563.

Wesely, M. L., Cook, D. R., Hart, R. L. and Speer, R. E. 1985. Measurements and parameterization of particulate sulfur dry deposition over grass. J. Geophys. Res. 90, 2131–2143.

Wyers, G. P. and Duyzer, J. H. 1997. Micrometeorological measurement of the dry deposition flux of sulphate and nitrate aerosols to coniferous forest. Atmos. Environ. 31, 333–343.

Zhang, L., Gong, S., Padro, J., & Barrie, L. (2001). A size-segregated particle dry deposition scheme for an atmospheric aerosol module. *Atmospheric environment*, **35**(3), pp.549-560.

Zhang, J. and Shao, Y., 2014. A new parameterization of particle dry deposition over rough surfaces. Atmospheric Chemistry and Physics, 14(22), pp.12429-12440.

Zhang, J., Shao, Y. and Huang, N. 2014. Measurements of dust deposition velocity in a wind-tunnel experiment. Atmos. Chem. Phys. 14, 8869–8882.

Zufall, M. J., Davidson, C. I., Caffrey, P. F. and Ondov, J. M. 1998. Airborne concentrations and dry deposition fluxes of particulate species to surrogate surfaces deployed in southern Lake Michigan. Environ. Sci. Technol. 32, 1623–1628.

Zhang, X., Lyu, J., Zeng, Y., Sun, N., Liu, C. and Yin, S., 2021. Individual effects of trichomes and leaf morphology on PM2. 5 dry deposition velocity: A variable-control approach using species from the same family or genus. Environmental Pollution, 272, p.116385.